JPE 19-5-3

https://doi.org/10.6113/JPE.2019.19.5.1087
ISSN(Print): 1598-2092 / ISSN(Online): 2093-4718

Analysis of Key Parameters for Inductively Coupled Power Transfer Systems Realized by Detuning Factor in Synchronous Generators

Jinfeng Liu†, Kun Li*, Ningzhi Jin*, and Herbert Ho-Ching Iu**

†,*Engineering Research Center of Automotive Electronics Drive Control and System Integration, Ministry of Education, Harbin University of Science and Technology, Harbin, China
**School of Electrical, Electronics and Computer Engineering, University of Western Australia, Perth, WA, Australia

Abstract

In this paper, a detuning factor (DeFac) method is proposed to design the key parameters for optimizing the transfer power and efficiency of an Inductively Coupled Power Transfer (ICPT) system with primary-secondary side compensation. Depending on the robustness of the system, the DeFac method can guarantee the stability of the transfer power and efficiency of an ICPT system within a certain range of resistive-capacitive or resistive-inductive loads. A MATLAB-Simulink model of a ICPT system was built to assess the system's main evaluation criteria, namely its maximum power ratio (PR) and efficiency, in terms of different approaches. In addition, a magnetic field simulation model was built using Ansoft to specify the leakage flux and current density. Simulation results show that both the maximum PR and efficiency of the ICPT system can reach almost 70% despite the severe detuning imposed by the DeFac method. The system also exhibited low levels of leakage flux and a high current density. Experimental results confirmed the validity and feasibility of an ICPT system using DeFac-designed parameters.

Key words: Detuning factor, Efficiency, ICPT, Resonant compensation, Rotary transformer, Transfer power

I. INTRODUCTION

Traditional direct point-to-point power transfer methods have been unable to satisfy the needs of certain special applications, notably in cases such as mining, underwater applications or locations with flammable materials [1]-[3]. There are other problems that cannot be avoided with this form of power transfer, e.g. grind and aging. A particular issue is that traditional power transfer processes tend to generate sparks, reducing the service-life of equipment and raising concerns about electrical safety [4]-[6]. As a safe, reliable and flexible alternative, inductively coupled power transfer (ICPT) technology has attracted considerable attention [7], [8]. Associated research has focused on matters such as the optimal design of mutual inductance parameters, system frequency characteristics [9], transfer power, transfer efficiency, compensation modes for the primary and secondary windings, and energy transfer distance.

Common methods for improving the power transfer capability of ICPT systems include increasing the working frequency or transfer power, and improving the quality of the resonant circuits or coupled coefficients. A maximum energy efficient product approach has been proposed [10]. The approach seeks to optimize the coupled parameters of the mutual inductance. This offers the possibility of meeting the needs of power transfer through the globally optimized design of an ICPT system. Some research has suggested [11], [12] that the frequency of a resonant system can be split if the distance between the coils in a multi-coil transfer structure is too close, which leads to multiple peaks in the efficiency-frequency curve. However, frequency splitting technology [13], [14] can offer frequency tracing compensation for different

Manuscript received Feb. 24, 2019; accepted Apr. 25, 2019
Recommended for publication by Associate Editor Dukju Ahn.
†Corresponding Author: ljf78118@163.com
Tel: +86-188-0368-8668, Fax: +86-451-86390354, HUST
*Engineering Research Center of Automotive Electronics Drive Control and System Integration, Ministry of Education, Harbin University of Science and Technology, China
**School of Electrical, Electronics and Computer Engineering, University of Western Australia, Australia

coil distances, which improves their transfer efficiency. Analyses of the working principles and potential system structures for contactless energy transfer [15]-[20] have presented a number of possible solutions for ICPT systems where different forms of compensation may be brought about on both the primary and secondary sides [21]. An examination of the calculation methods for ICPT transfer power and efficiency [22] suggests that the over-coupling range results are inconsistent with the goals of maximum power and maximum efficiency when frequency splitting occurs.

All of these approaches have a similar problem, i.e., they do not fully compensate the issues of robustness in inductively coupled systems when some of the factors are changed. As ICPT technology advances, more and more electrical devices will use contactless power supplies in the future [23]-[26]. This will lead to an emphasis not only upon the quality and reliability of such systems, but also upon their power and efficiency. Simply increasing the operating frequency has increased the power requirements of ICPT systems, while existing frequency conversion technologies cannot guarantee any working frequency [10]. Moreover, improving transfer power at the expense of system efficiency is not a sustainable proposition. Some research [1] indicates that a larger coupled coefficient does not necessarily improve ICPT power. As a result, there is a need for further research on this topic. One thing that is clear is that a better match between ICPT power and efficiency can be achieved if the quality of the resonant circuits is increased.

The core problem in robustness design is optimization. In engineering, optimized design seeks to find specific optimal solutions within constrained feasible regions [27], [28]. Various researchers have analyzed the parameters in ICPT systems. However, to date they have only discussed compensation capacitance in relation to the resistive load in systems, without looking at resistive-capacitive, resistive-inductive or variable loads [29]. Moreover, capacitance compensation results are complex, which may limit the applicability of ICPT technology in certain cases. Over-coupling is different from under-coupling in ICPT since the maximum power distribution and the maximum efficiency distribution may be at odds [22]. To maintain robustness, a detuning factor correction method (DeFac), which is a parameter design method tailored for ICPT systems, can offer a solution to the problem of over-coupling.

A DeFac approach takes the mismatch between power and efficiency into account under ICPT over-coupling. The distribution of power and efficiency is analyzed regardless of whether the load is resistive-inductive, resistive-capacitive or variable. In order to compare the capability of transfer power, the maximum power ratio (PR) is applied, which is the proportion of the load power to the rated load power of the maximum power method. This DeFac method can ensure that the maximum PR and efficiency both reach almost 70% when the ICPT is detuning. In this paper, an ICPT system for excitation in a synchronous generator is used as an example to illustrate use of the DeFac approach for resonant compensation circuits.

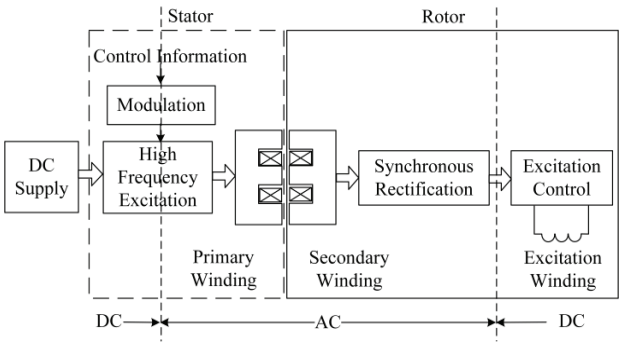

Fig. 1. Excitation energy inductively coupled system.

II. An ICPT System for Excitation in a Synchronous Generator

Excitation energy inductively coupled systems are composed of a high-frequency DC-AC converter, a loosely coupled rotary transformer, an AC-DC converter and an excitation winding. In synchronous generators, an isolated DC-DC converter is used in the internal high-frequency power supply switch and a loosely coupled rotary transformer can replace the collector ring and brush used in traditional excitation systems to achieve brushless excitation. An overall block diagram of the system is shown in Fig. 1. The inverter can change the DC input from the power supply to high-frequency AC power through switches controlled by a high-frequency pulse width modulation (PWM) signal. The converted high-frequency AC power is then transferred to the primary coil of the loosely coupled rotary transformer. The inductive high-frequency voltage on the secondary side is rectified and filtered to an excitation winding. The secondary winding of the loosely coupled rotary transformer and the rotor of the synchronous generator are arranged in the same axis. As a result, the magnetic circuit is almost unaffected by use of the loosely coupled rotary transformer when the secondary iron core rotates with the rotor. In this way, defects caused by the wear of both the collector ring and brush in traditional power systems are completely eliminated.

An assembly diagram of the excitation energy inductively coupled system is shown in Fig. 2. The secondary core and rectifier of the loosely coupled rotary transformer are aligned with the motor rotor core and the excitation winding. The other parts, including the controller and the inverter, are installed on the stator of the synchronous generator. The primary core of the transformer is fixed at the end of the motor stator and is opposite the secondary core. The air gap between the primary and secondary cores is at a controlled distance of between 0.5 and 1.5 mm [30].

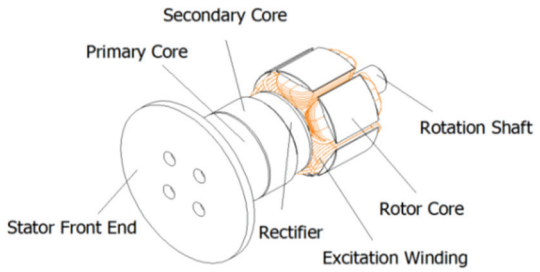

Fig. 2. Assembly of an inductively coupled system.

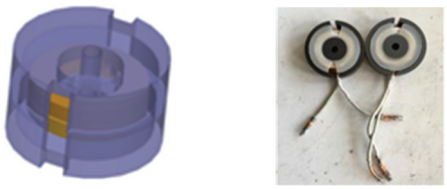

(a) (b)

Fig. 3. Separable magnetic tank transformer. (a) Simulation. (b) Physical structure.

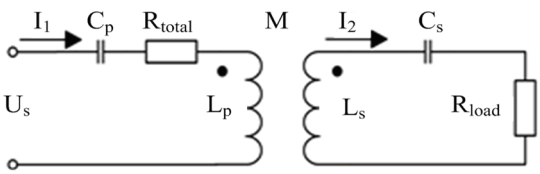

Fig. 4. ICPT series compensation topology showing the primary and secondary sides.

The core component of the ICPT is the separable rotary transformer, which takes advantage of the fact that the energy transfer of the magnetic tank transformer is not affected by the rotary speed when the primary and secondary sides maintain relative rotation. Fig. 3 shows a simulation and the actual physical structure of the separable magnetic tank transformer.

III. Series Resonant Compensation of the Primary and Secondary Sides of the ICPT

A. Series Resonant Compensation Topology

A series resonant compensation topology of the primary and secondary windings of the ICPT is shown in Fig. 4.

L_P and L_S represent the primary and secondary winding inductances, respectively. C_P and C_S represent the compensation capacitance of the primary and secondary sides, respectively. R_{total} represents the sum of the power supply resistance and the primary winding, and R_{load} represents the resistance of the load. M represents the mutual inductance [31]. I_1 and I_2 are the winding currents of the primary and secondary sides, respectively.

Since the resistance of the secondary winding is much lower than the resistance of the load, it has little effect on the transfer power. For the convenience of analysis, it is possible to omit the secondary winding resistance. The equivalent equations can be expressed as follows:

$$\begin{cases} R_p = R_{load} = R \\ L_p = L_s = L \\ C_p = C_s = C \end{cases} \tag{1}$$

From this, Kirchoff's Voltage Law (KVL) equations for the ICPT circuit can be obtained as follows:

$$U_S = (R + j\omega L + \frac{1}{j\omega C})I_1 - j\omega M I_2 \tag{2}$$

$$(R + j\omega L + \frac{1}{j\omega C})I_2 - j\omega M I_1 = 0 \tag{3}$$

If it is supposed that ξ is the generalized detuning factor, and δ is the coupling factor, the corresponding functional relationships can be defined as follows [12], [29]:

$$\xi = Q(\frac{\omega}{\omega_0} - \frac{\omega_0}{\omega}) \tag{4}$$

$$\delta = \frac{\omega M}{R} \tag{5}$$

$$Q = \frac{\omega_0 L}{R} = \frac{1}{\omega_0 C R} \tag{6}$$

where Q represents the quality factor, ω represents the working angular frequency, and ω_0 represents the natural angular frequency. α is the maximum PR of the load, and η is the transfer efficiency of the ICPT. The corresponding functional relationships can now be defined as follows [29]:

$$\alpha = \frac{4\delta^2}{(1 - \xi^2 + \delta^2)^2 + 4\xi^2} \tag{7}$$

$$\eta = \frac{\delta^2}{\sqrt{\xi^2\left[\left(\xi^2 - \delta^2\right)^2 + 3\left(1 + \xi^2\right)\right] + \left(1 + \delta^2\right)^2}} \tag{8}$$

MATLAB 3D simulation images of the maximum PR and power efficiency are shown in Fig. 5. It can be seen from Figs. 5(a) and (b) that there is an over-coupling mismatch between the power and the efficiency. For example, when the detuning factor is 1.53 and the coupling factor is 5.09, the efficiency reaches 57.3%. However, the power only reaches 16.9% of the maximum PR. Fig. 5(c) shows that the peak sum of the maximum PR and efficiency is around 1.55. This implies that an increase of one aspect, either the maximum PR or the efficiency, inevitably leads to a decrease in the other. In other words, they are mutually restrictive.

Fig. 6 provides a common solution set for when, according to Fig. 5, the maximum PR and the transfer efficiency are both greater than 60%. If the coupling factor falls to between 1.2 and 2.8 higher values of maximum PR and efficiency are guaranteed. This can be verified by the following calculation in section 3.2. If the detuning factor ξ and the coupling factor δ are in regions I and II in Fig. 6 after the load changes, the

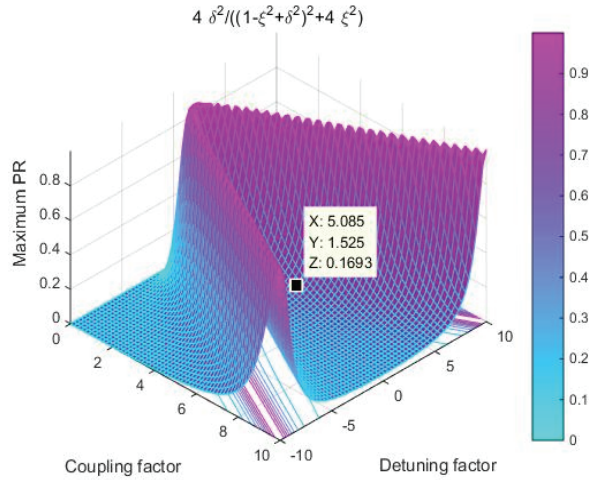

(a)

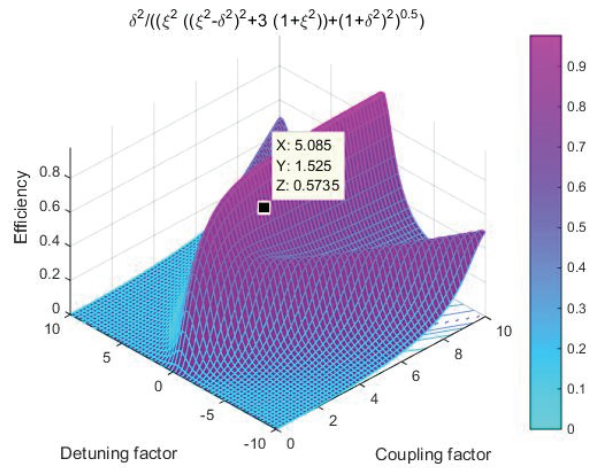

(b)

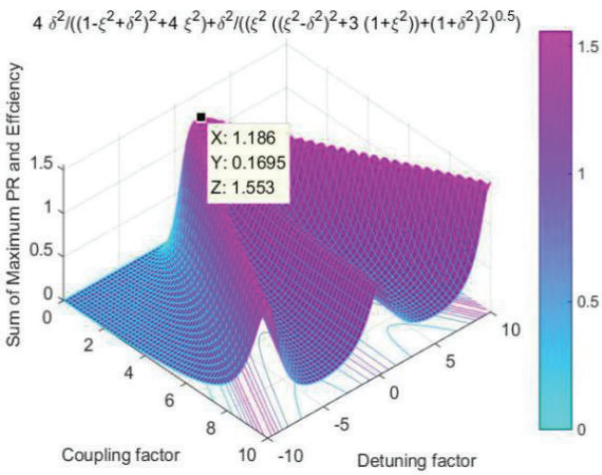

(c)

Fig. 5. 3D simulations of the maximum PR and transfer efficiency. (a) Maximum PR. (b) Transfer efficiency. (c) Sum of the maximum PR and efficiency.

parameters of the ICPT system avoid the unreasonable solution presented in Fig. 5, and achieve a much better match between the load power and efficiency.

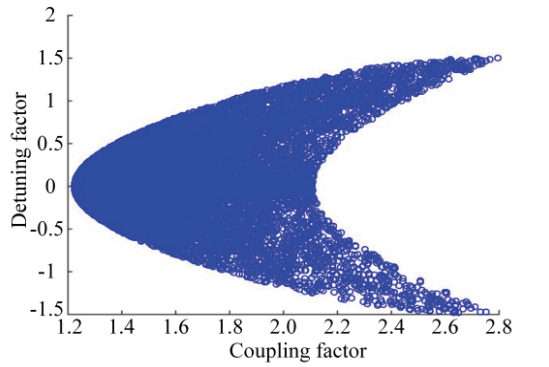

(a)

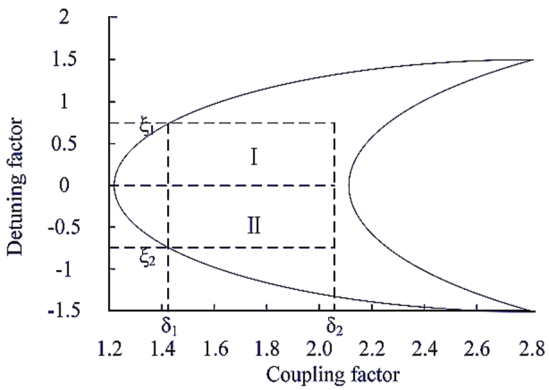

(b)

Fig. 6. Common solution set when the maximum PR and efficiency are both above 60%. (a) Scatter diagram. (b) Regional diagram.

B. Design of Compensation Parameters by the Detuning Factor Correction Method

According to the characteristics of ξ itself, its absolute value represents a deviation between the working frequency and resonant frequency of the ICPT. A negative value shows that the working frequency is below the ICPT resonant frequency. Meanwhile, a positive value shows that the working frequency is above the resonant frequency of the system. L represents the initial inductance of the ICPT with a resistive load. This enables the determination of the working angular frequency ω. Lv represents the variational inductance of the ICPT after the load changes. This allows for the determination of the natural angular frequency ω_0. On this basis, ξ can be obtained from (4) and (6) as follows:

$$\begin{aligned}\xi &= \frac{L_v}{R}\left(\omega - \frac{\omega_0^2}{\omega}\right) \\ &= \frac{L_v}{R}\left(\frac{1}{\sqrt{LC}} - \frac{1}{L_v C}\sqrt{LC}\right)\end{aligned} \tag{9}$$

Thus, ξ can determine the deviation between ω and ω_0. L_v can be derived from (9) when the load changes:

$$L_v = \xi R\sqrt{LC} + L \tag{10}$$

When ξ is positive, $L_v > L$, which is equivalent to the inductive load. When ξ is negative, $L_v < L$, i.e., the secondary

circuit impedance is decreasing, which is equivalent to the capacitive load. In this case, the inductive load can be estimated as follows:

$$L_{load} = \xi R\sqrt{LC} \tag{11}$$

According to (5), the resistive load can be obtained using the following equation, where K represents the coupled coefficient of the transformer:

$$R_{load} = \frac{\omega M}{\delta} = \frac{K\sqrt{L}}{\delta\sqrt{C}} \tag{12}$$

where K=M/L and $\omega = 1/\sqrt{LC}$. Drawing upon (11) and (12), L can be expressed as follows:

$$L = \frac{L_{load}\delta}{K\xi} \tag{13}$$

The decrement of the inductance ΔL can be derived from (10) when the capacitive load is introduced into the system:

$$\Delta L = \xi R\sqrt{LC} \tag{14}$$

Therefore, the equivalent capacitive load can be derived from the following equations:

$$\frac{1}{\omega C_{load}} = \omega\Delta L \tag{15}$$

$$C_{load} = \frac{\sqrt{LC}}{\xi R} \tag{16}$$

From the above equations, it can be seen that the inductive load L_{load}, resistive load R_{load}, capacitive load C_{load}, and initial inductance L are all related to the detuning factor ξ. Fig. 6 shows that, for the resistive-inductive load, there is an area of resistive load and inductive load in region I once L and K are determined. Note the maximum PR of the load and the efficiency are above 60% at any load within this area. For the resistive-capacitive load, there is an area of resistive load and capacitive load in region II. Any load in this area can achieve a maximum PR and efficiency above 60%.

On this basis, the initial inductance L and compensation capacitance C for the resistive-inductive load of the ICPT can be acquired by the following equations:

$$L = \frac{L_{\max}\delta_2}{K\xi_2} \tag{17}$$

$$C = \frac{KL_{\max}}{\delta_2 R_{\min}^2\xi_2} \tag{18}$$

where R_{min} represents the minimum resistive load and L_{max} represents the maximum inductive load if the load margin is taken into account. Otherwise, R_{min} represents the load resistance and L_{max} represents the load inductance.

For the resistive-capacitive load of the ICPT, the initial inductance L and compensation capacitance C are as follows:

$$L = \frac{R_{\max}^2\delta_1^2 C_{\min}|\xi_1|}{K} \tag{19}$$

$$C = \frac{C_{\min}|\xi_1|K}{\delta_1} \tag{20}$$

where R_{max} represents the maximum resistive load and C_{min} represents the minimum capacitance load if the load margin is taken into account. Otherwise, R_{max} represents the load resistance and C_{min} represents the load capacitance.

When there is some allowance for the areas covered by regions I and II in Fig. 6, the DeFac method is a conservative design method. Nevertheless, the stability of an actual ICPT is superior to the requirements given by the pre-design.

IV. Comparison of Approaches to ICPT Parameter Design

A. Different Methods for Compensation Parameter Design

At present, the principal methods used to design ICPT parameters, including the compensation inductance, capacitance, and mutual inductance, are Maximum Power (MaxP), Impedance Matching (IMatch), and Optimum Energy Efficiency Product (OEE). MaxP focuses on load power, with the goal of increasing the maximum PR to 1. The transfer efficiency of an ICPT is massively influenced by its system parameters. As a result, the parameters have to be constantly adjusted to ensure system efficiency. IMatch is also designed to maximize the load power. However, the transfer efficiency of the power supply when using this method is only able to reach 50%. OEE focuses on optimization of the coupled mutual inductance coefficient. In addition, it introduces an energy-efficiency product index into the system. Using this index, the coupled mutual inductance parameters can be optimized by reducing the maximum PR. Thus, the overall efficiency of the ICPT is improved.

However, the purpose of the DeFac approach is to obtain a good match between the transfer power and the efficiency. This pays attention to the influence of load disturbance on the power and efficiency of the system. Within a certain range of resistive load, resistive-inductive load or resistive-capacitive load, the efficiency and power ratio can be kept above 60% using this method.

To enable an effective experimental contrast, various parameters were simulated in as consistent a manner as possible using an experimental platform. The resistance was 3Ω since this was the resistance of the excitation winding in the experimental platform developed for a synchronous generator. The resistive load offset was 0.5Ω and the maximum inductive load offset was 1 mH. The input voltage amplitude was 24V and the MOSFET switching frequency was 200kHz. For the sake of comparison and analysis, the reference maximum PR of the 3Ω load was 24W. The ICPT system parameters for each of the methods are given in Table I, where it was given that K = 0.7 and Rtotal = R = 3Ω.

B. Simulation Analysis Using MATLAB

Fig. 7 shows a simulated model of an inductively coupled excitation energy system with a resonant compensation circuit.

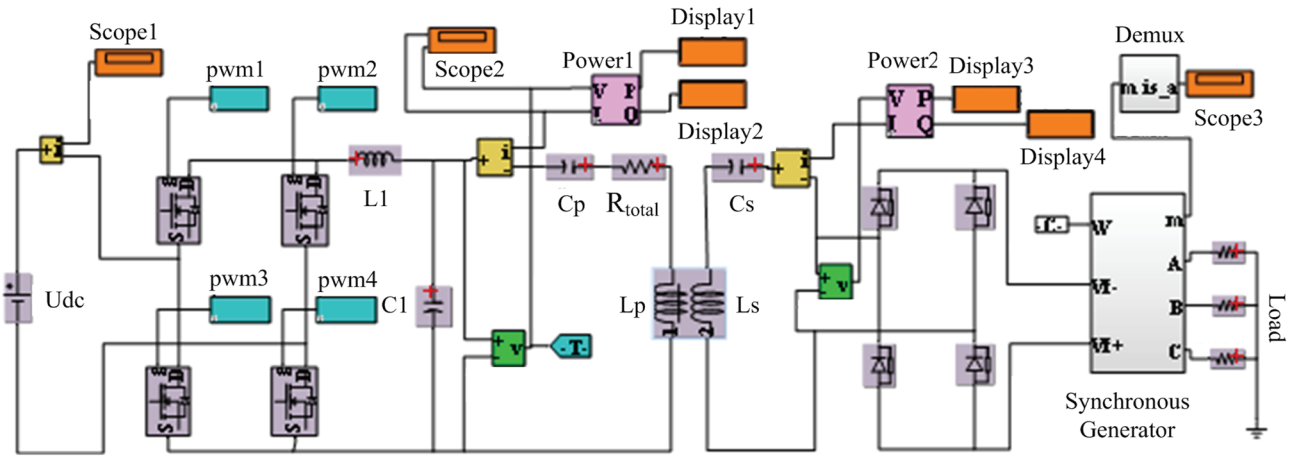

Fig. 7. Simulation of an inductively coupled excitation energy system.

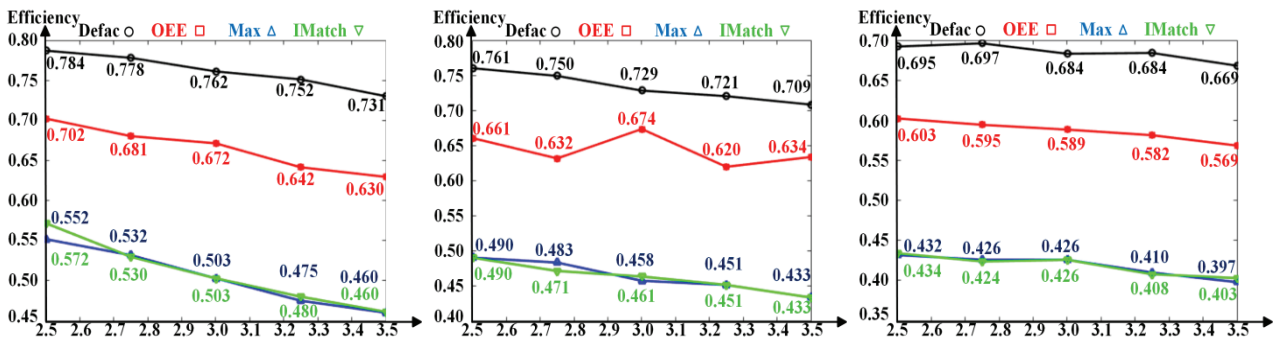

Fig. 8. Efficiency scatter diagrams with different load characteristics. (a) Resistive load (2.5Ω≤R≤3.5Ω). (b) Resistive-inductive load (2.5Ω≤R≤3.5Ω and inductive = 1 mH). (c) Resistive-capacitive load (2.5Ω≤R≤3.5Ω and capacitive=420 μF).

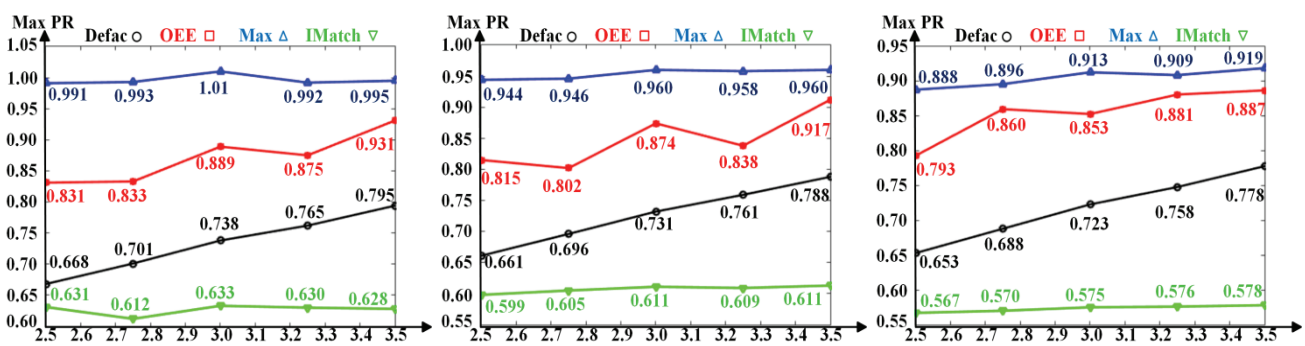

Fig. 9. Max PR scatter plots with different load characteristics. (a) Resistive load (2.5Ω≤R≤3.5Ω). (b) Resistive-inductive load (2.5Ω≤R≤3.5Ω and inductive = 1 mH). (c) Resistive-capacitive load (2.5Ω≤R≤3.5Ω and capacitive=420 μF).

The values of the simulation parameters were set to the results shown in Table I. The first stage SPWM inverter needs to be able to generate AC voltage. This enables the efficiency and maximum PR to be acquired using a variety of methods.

Fig. 8 and 9 show a comparison of simulation results for the four methods with different load characteristics. It can be seen that the efficiency and maximum PR of the ICPT designed using DeFac are about 70%. Furthermore, in Fig. 8, the maximum loss breakdown of DeFac for the three different load characteristics are 5.7%, 5.2% and 2.8%, respectively. They are all lower than those of OEE (7.2%, 5.4% and 6.4%), MaxP (9.2%, 6.3% and 3.5%) and IMatch (11.2%, 6.3% and 3.1%). For MaxP, the maximum PR is close to 100%. However, the efficiency is only 50%. For IMatch, the efficiency and maximum PR of the ICPT are lower than those of DeFac. For OEE, the efficiency with a nominal load only reaches 66.7%. As can be seen, for the resistive-inductive load, the variations in DeFac's maximum PR and efficiency

TABLE I
DESIGN PARAMETERS OF THE ICPT SYSTEM ACCORDING TO DIFFERENT METHODS

Method	Nomenclature	Value
DeFac	ξ	0.5
	L	6 mH
	C	105 μF
	M	4.2 mH
Imatch	L	6 mH
	C	105 μF
	M	4.2 mH
MaxP	L	3.4 mH
	C	186 μF
	M	2.39 mH
OEE	L	4.82 mH
	C	131 μF
	M	3.37 mH

were less than 1% and 4% corresponding the resistive load. These are smaller than the values for OEE, IMatch and MaxP. For the resistive-capacitive load, DeFac's maximum PR and efficiency variation was less than 2% and 9% corresponding resistive load, which is again smaller than the others.

From the results shown in Fig. 8 and 9, it is clear that the transfer efficiency of the ICPT designed by the DeFac correction method is superior to that of the others since it takes both the maximum PR and efficiency into consideration. Although its maximum PR is lower than that of the others, this only represents the demand for the voltage amplitude of the power supply. By comparing the maximum PR for different loads using the same method, it is easy to see that the maximum PR of the ICPT remains largely unchanged when the parameters were designed using DeFac, which ensures power stability. Indeed, for the ICPT designed using DeFac, if the amplitude of the supply voltage is increased by 20%, a similar load power to MaxP is obtained, whilst retaining a much higher efficiency.

Obviously, if the voltage amplitude is increased by 20%, an improved power supply is required and the ICPT components need to be improved. For most applications, this is not a difficult requirement to meet. In such cases, efficiency should be the top priority when the power supply voltage requirements are not too strict.

The OEE and DeFac methods are the main comparison methods in the following experiments. Therefore, Fig. 10 shows the primary voltage and current of the transformer when the resonant parameters are obtained by OEE and DeFac. It is obvious that DeFac has a smoother primary voltage. Meanwhile, the amplitude of the primary current is about 1.5A for OEE. However, that is up to 1.8A for DeFac. It is demonstrated that DeFac has a better resonance compensation effect than OEE.

Fig. 11 shows output voltage waveforms of the synchronous generator for four different methods. The voltage amplitude of DeFac is lower than of OEE and MaxP since the maximum PR obtained by DeFac is lower than that obtained by OEE and MaxP. This is due to the fact that DeFac takes the need for a higher efficiency into consideration.

Fig. 12 shows the AC output voltages of a generator at

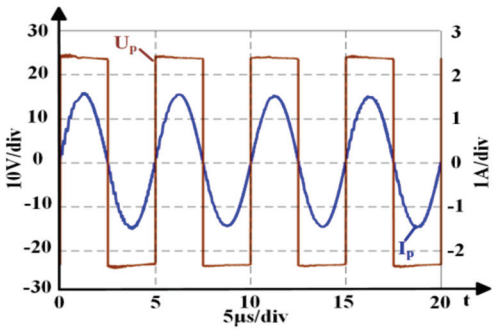

(a)

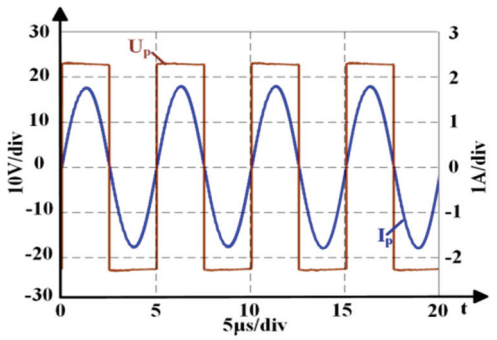

(b)

Fig. 10. Primary voltage and current of a transformer. (a) OEE. (b) DeFac.

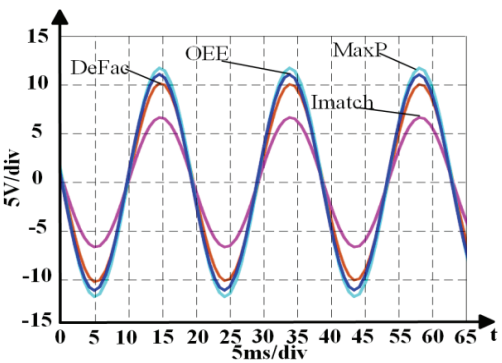

Fig. 11. Synchronous generator output voltage waveforms for four different methods.

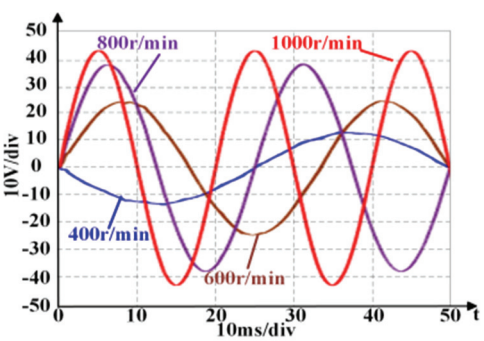

Fig. 12. Synchronous generator output voltage waveforms at different speeds.

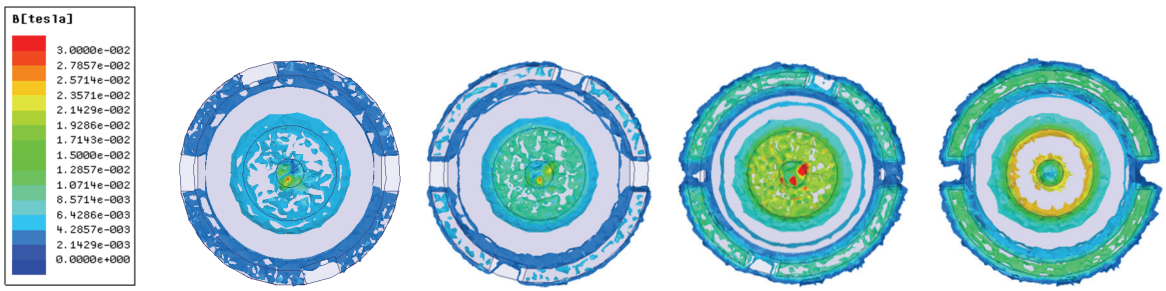

(a) (b) (c) (d)

Fig. 13. Leakage flux density distribution of a contactless transformer according to four different methods. (a) DeFac. (b) OEE. (c) MaxP. (d) IMatch.

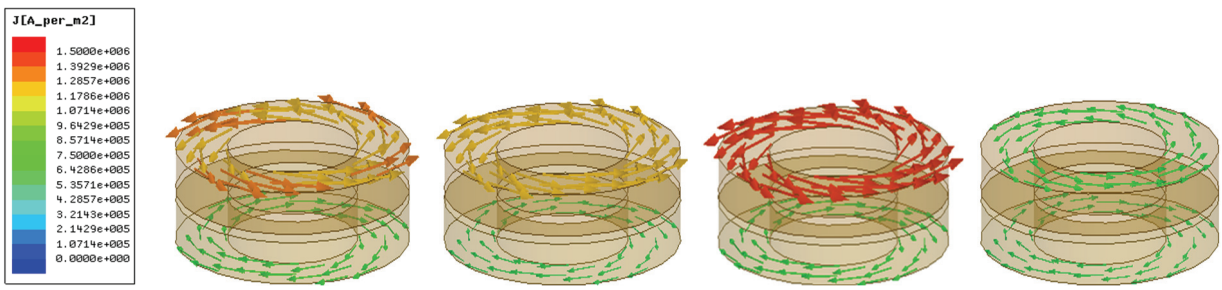

(a) (b) (c) (d)

Fig. 14. Current density distribution of a contactless transformer according to four different methods. (a) DeFac. (b) OEE. (c) MaxP. (d) IMatch.

different speeds. The amplitude and frequency of the voltage increase with the speed. When the rated speed is reached, the amplitude of the output voltage is stable at about 40V.

C. Simulation Analysis Using Ansoft

Since it forms a core part of contactless inductively coupled excitation systems, it was necessary to build an Ansoft Maxwell 3D simulation model of a separable magnetic tank transformer and to analyze its electromagnetic relative rotation performance. Therefore, its mutual inductance was modeled and analyzed for the four different methods.

In a contactless synchronous generator rotor excitation system, the primary side of the magnetic tank transformer has a ±24V square wave, with a working frequency of 200 kHz. This standard was used to establish the excitation source of the 3D simulation model. The turn ratio of the transformer was 1:1. The simulation experiment was conducted when the primary and secondary side of the transformer were in a relative state of rotation, i.e., the primary side was still at rest and the speed of the secondary side was 1200r/min. The resistive load was 3Ω and transient simulation results were intercepted at a simulation time of 6ms. Fig. 13 shows a series of cloud diagrams of the leakage flux distribution for the magnetic tank transformer according to the four parameter design methods. It can be clearly seen that the leakage flux was very large because of the air gap between the primary and secondary side, which makes the magnetic field diverge. This is the principal reason for the low transfer efficiency of ICPT. From Fig. 9, it can be seen that the leakage flux of the central axis determined by MaxP was the highest, while that determined by DeFac was the lowest. This suggests that DeFac is relatively efficient.

Fig. 14 shows the current density distribution of the transformer with the four methods. To facilitate the observation of the winding current density distribution of the transformer, the magnetic core model was omitted from the simulation results. It can be seen from the results that the current density of the primary winding was larger than that of the secondary winding. It can also be seen that there is a notable temperature problem due to the current density when the transformer was in use. Comparing the results for the four methods, the largest current density was not generated when the system parameters were determined by DeFac. However, it had the lowest current density loss between the primary and secondary winding. Therefore, the transfer efficiency and the PR were both higher when using DeFac.

V. Experimental Verification

To verify the effectiveness of DeFac, an experimental ICPT platform, based on an IR2110 driver, was set up in a laboratory. The experimental platform consisted of three parts including the motor, a synchronous generator, and a contactless coupled excitation energy system, i.e., an ICPT. The ICPT excitation system was the core of the experimental platform, which provided the magnetic field for the synchronous

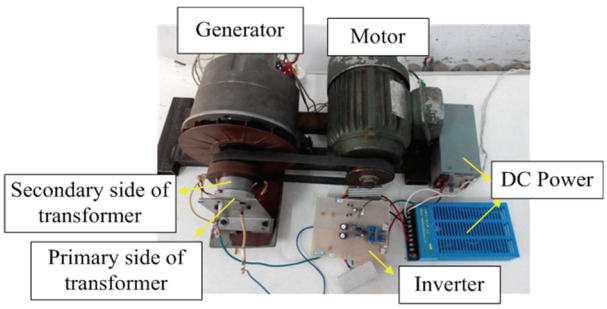

Fig. 15. Experimental excitation system platform with a separable transformer.

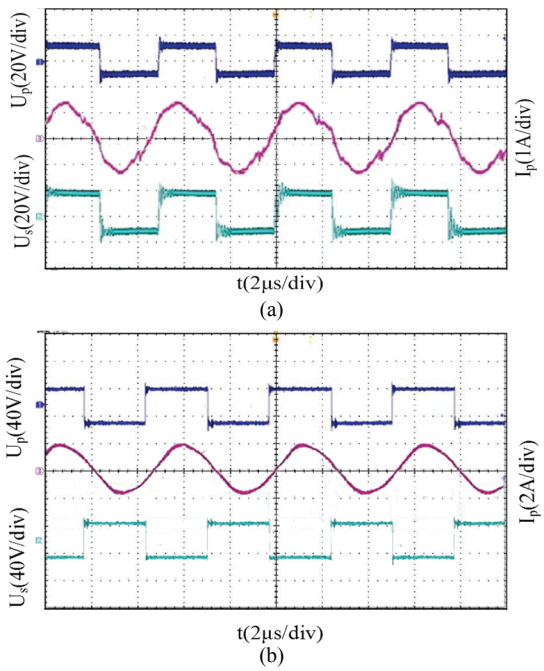

Fig. 16. Contrasting output waveforms generated by two different methods. (a) OEE. (b) DeFac.

generator. Fig. 15 shows the experimental platform with a separable magnetic tank transformer for the contactless excitation system in the relative rotary state. The primary side is fixed on the base, and the secondary side with rectification is fixed on the shaft of the rotor.

Within the platform, an excitation square wave of ± 24 V and 200 kHz was provided by an inverter circuit with an IR2110 for the primary winding of the separable magnetic tank transformer. The secondary core of the transformer was connected to the coaxial axis of the motor rotor and the square wave from the primary side was sent to a rectifier device. The rectifier circuit rotated coaxially with the generator rotor. The air gap between the primary and secondary sides of the transformer, the rotary speed of the secondary side and the frequency of the power supply were all adjustable. Fig. 16 shows the primary and secondary winding output voltages and primary current waveforms of a transformer fabricated with parameters corresponding to the OEE and DeFac methods (provided in Table I) when the system was static.

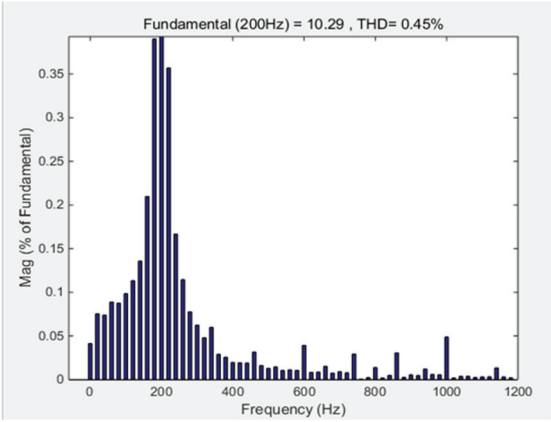

Fig. 17. Fourier transform results of output waveforms of the generator for two different methods. (a) DeFac. (b) OEE.

Because there was leakage inductance in the primary part of the transformer, it along with the distributed capacitance of the MOSFET form ringing voltage by oscillating. In Fig. 16(a), the resonance parameters designed by OEE caused the ringing voltage, to a certain extent, on the primary side of the transformer. In addition, the transfer current was distorted. However, in Fig. 16(b), the primary and secondary series capacitance designed by DeFac compensated the leakage inductance of the transformer by the resonance. Therefore, the ringing voltage was reduced and the voltage and current waveforms were smoother and higher than the former, which is consistent with the simulation results in Fig.10. In the end, the DeFac method improved both the output effect and the transfer capability.

Fig. 17 shows Fourier transform results of the output waveforms of the generator using the DeFac and OEE methods. The total harmonic distortion (THD) for the DeFac method was noticeably smaller than it was for the OEE. The final THD of the output waveform of the synchronous generator was only 0.45%.

Fig. 18 shows output voltage waveforms for two methods. The voltage amplitude for the DeFac method is lower than it is for the OEE method, which is in agreement with the

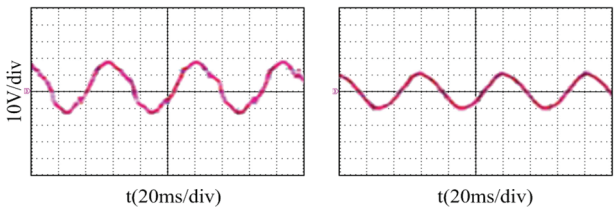

Fig. 18. Contrasting generator output voltage waveforms for two different methods. (a) OEE. (b) DeFac.

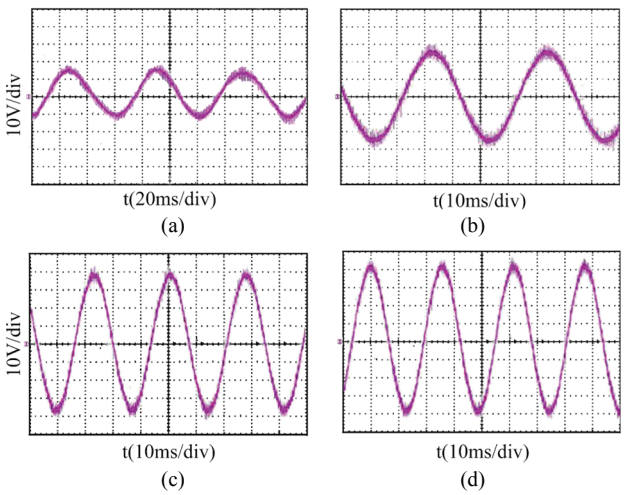

Fig. 19. Output voltage waveform of a synchronous generator at different speeds. (a) 400 r/min. (b) 600 r/min. (c) 800 r/min. (d) 1000 r/min.

simulation results shown in Fig. 11. However, the obtained output voltage waveform of the contactless transformer designed by OEE is aberrant, whilst that generated by DeFac is much smoother.

The principal motor, which was controlled by the frequency converter, was able to drive the synchronous generator to generate electricity. The output AC voltage provided a further way of verifying the performance of the proposed method. Fig. 19 shows the output voltage at different speeds. The output voltage was relatively low at a lower rotational speed. When the rotational speed exceeded 1000 rpms, the voltage waveform was smoother and more stable than it was at lower rotational speeds, which is consistent with the primary excitation effect of the generator itself. Meanwhile the amplitude and frequency variation are basically consistent with the simulation result in Fig. 12. This shows that an ICPT using the parameters provided by the DeFac method is effective at bringing about an excitation effect in AC synchronous generators.

From the obtained experimental results, it can be seen that the current of the stator winding in the generator can be varied when the generator load is changed. Thus, the armature reaction leads to variations in the combined magnetic field, which results in variations in the outlet voltage of the generator. The outlet voltage of the generator can be collected to realize

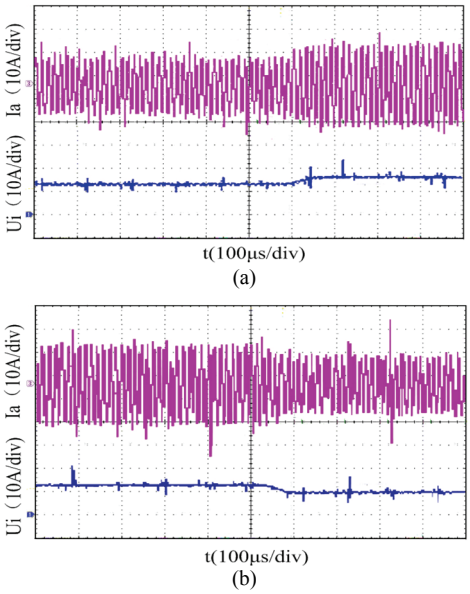

Fig. 20. Change in the output phase current with the input DC voltage Ui for different statuses. (a) Increasing voltage. (b) Decreasing voltage.

a closed-loop excitation system through the sinusoidal pulse width modulated (SPWM) control of metal oxide semiconductor field-effect transistors (MOSFETs). This is something that will be addressed in future research.

To further verify the dynamic performance of the synchronous generator, the input DC voltage of the wireless power transfer system was changed to directly influence the excitation current. The corresponding experimental results are presented in Fig. 20. The single-phase output current (Ia) of the synchronous generator was able to change with the input DC excitation voltage (Ui). This is the same as it would be with a traditional synchronous generator, which validates the effectiveness of the wireless excitation power transfer.

VI. Conclusion

In this paper, a Detuning Factor (DeFac) method was proposed for the design of ICPT parameters. A simulation was used to compare the effectiveness of the proposed method with three other methods, i.e., MaxP, OEE and IMatch. The efficiency and maximum PR provided by the DeFac method approached 70%, which exceeds the performance offered by the other three methods. The stability of the PR according to different load properties, such as resistive-inductive or resistive-capacitive, was also superior. In addition, the load power is guaranteed.

The proposed ICPT parameter design method can provide the key parameters for efficient calculations, including the capacitance, the compensation inductance and the mutual inductance of the transformer. The DeFac method can achieve an efficiency of almost 70% and the maximum PR at the same time.

ACKNOWLEDGMENT

The authors gratefully acknowledge the financial support of Natural Science Foundation of Heilongjiang Province of China to Guide the Project (No. LH2019E067) and Innovative Talents of Science and Technology of Harbin, China (No.2016 RAQXJ018).

REFERENCES

[1] C. Fang, X. F. Li, Z. M. Xie, and J. Y. Xu, "Design and optimization of an inductively coupled power transfer system for the underwater sensors of ocean buoys," *Energies*, Vol. 10, No. 1, pp. 23-32, Jan. 2017.

[2] M. W. Lin, D.J. Li, and C. J. Yang, "Design of an ICPT system for battery charging applied to underwater docking systems," *Ocean Eng*., Vol. 145, pp. 373-381, Nov. 2017.

[3] J. T. Boys, G. A. Covic, and G. A. J. Elliott, "Pick-up transformer for ICPT applications," *Electron. Lett*., Vol. 38, No. 21, pp. 1276-1278, Oct. 2002.

[4] M. Y. Yang, P. Wang, Y. Z. G, and Z. F. Yang, "Models and experiments for the main topologies of MRC-WPT systems," *J. Power Electron.*, Vol. 17, No. 6, pp. 1694-1706, Nov. 2017.

[5] K. Keisuke, "Development trend of inductive power transfer systems with focus on transmission frequency and transmission power," *IEEJ Trans. Ind. Appl*, Vol. 137, No. 5, pp. 445-457, Feb. 2017.

[6] A. Dukju and H. Songcheol, "A study on magnetic field repeater in wireless power transfer," *IEEE Trans. Ind. Electron*., Vol. 60, No. 1, pp. 360-371, Apr. 2013.

[7] H. Z. Z. Beh, G. A. Covic, and B. John, "Wireless Fleet Charging System for Electric Bicycles," *IEEJ. Emerg. Sel. Top. Power Electron.*, Vol. 3, No. 1, pp. 75-86, Mar. 2015.

[8] C. S. Wang, O. H. Stielau, and G. A. Covic., "Design considerations for a contactless electric vehicle battery charger," *IEEE Trans. Ind. Electron*., Vol. 52, No. 5, pp. 1308-1314, Oct. 2005.

[9] X. Li, Y. Sun, Z. H. Wang, and C. S. Tan, "Development of current-fed ICPT system with quasi sliding mode control," *WSEAS Trans. Circuits Syst*., Vol. 11, No. 11, pp. 351-360, Nov. 2012.

[10] Y Sun, C. Y. Xia, X. Dai, and Y. G. Su, "Analysis and optimization of mutual inductance for inductively coupled power transfer system," *Proc. the CSEE*, Vol. 30, No. 33, pp. 44-55, Nov. 2010.

[11] X. Zhang, Q. X. Yang, and H. Y. Chen, "Research on characteristics of frequency splitting in electromagnetic coupling resonant power transmission systems," *Proc. the CSEE*, Vol. 32, No. 9, pp. 167-173, Mar. 2012.

[12] Y. Li, Q. X. Y, Z. Yan, and H. Y. Chen, "Characteristic of frequency in wireless power transfer system via magnetic resonance coupling," *Electric Machines and Control*, Vol. 16, No. 7, pp. 7-11, Jul. 2012.

[13] N. Y. Kim, K. Y. Kim, and C. W. Kim, "Automated frequency tracking system for efficient mid-range magnetic resonance wireless power transfer," *Microwave Opt. Technol. Lett*., Vol. 54, No.6, pp. 1423-1426, Jun. 2012.

[14] Y. Li, Q. X. Yang, Z. Yan, and C. Zhang, "Analysis on effective range of wireless power transfer and its impact factors," *Diangong Jishu Xuebao*, Vol. 28, No. 1, pp. 106-122, Jan. 2013.

[15] R. K. M, Y. R. Lin, and Y. Li, "An active-rectifier-based maximum efficiency tracking method using an additional measurement coil for wireless power transfer," *IEEE Trans. Power Electron*., Vol. 33, No. 1, pp. 716-728, Jan. 2018.

[16] M. C. Yan, X. D. Wang, J. F. Liu, and Y. Yu, "Analysis of contactless excitation power supply resonance compensation," *Electric Machines and Control*, Vol. 19, No. 3, pp. 45-53, Mar. 2015.

[17] E. R. Joy, B. K. Kushwaha, G. Rituraj, and P. Kuma, "Analysis and Comparison of four compensation topologies of contactless power transfer system," in *Int. Conf. Electr. Power Energy Convers. Syst*., *EPECS*, pp. 1-6, 2015.

[18] Y. J. Wang, Y. S. Yao, X. S. Liu, and D. G. Xu, "An LC/S compensation topology and coil design technique for wireless power transfer," *IEEE Trans. Power Electron*., Vol. 33, No. 3, pp. 2007-2025, Mar. 2018.

[19] X. Liu, W. M. Ng, C. K. Lee, and S. Y. Hui, "Optimal operation of contactless transformers with resonance in secondary circuits," in *Conf. Proc. IEEE Appl. Power Electron. Conf. Expo*., *APEC*, pp. 645-650, 2008.

[20] M. Hedieh and M. Axel, "Design metrics of compensation methods for contactless charging of electric vehicles," in *Euro. Conf. Power Electron. Appl., EPE ECCE Europe*, pp. 1-10, 2017.

[21] H. H. Wu, G. A. Covic, J. T. Boys, and D. J. Robertson, "Series-tuned inductive-power-transfer pickup with a controllable AC-voltage output," *IEEE Trans. Power Electron*., Vol. 26, No. 1, pp. 98-109, Aug. 2011.

[22] J. Hua, H. Z. Wang, Y. Zhao, and A. L. Zou, "LCL resonant compensation of movable ICPT systems with a multi-load," *J. Power Electron*., Vol. 15, No.6, pp. 1654-1663, Nov. 2015.

[23] Y. J. Luan, B. Lin, and Q. Yang, "Effect of temperature and radial force on the transmission performance of contactless power transfer for rotary ultrasonic grinding," *IET Eletr. Power Appl.*, Vol. 11, No. 7, pp. 1169-1176, Aug. 2017.

[24] C. Auvigne, P. Germano, D. Ladas, and Y. Perriard, "A dual-topology ICPT applied to an electric vehicle battery charger," in *Proc. Int. Conf. Electr. Mach*, pp. 2287-2292, 2012.

[25] A. Momeneh, M. Castilla, I. M. M. Ghahderjan, and J. Miret, "Analysis, design and implementation of a residential inductive contactless energy transfer system with multiple mobile clamps," *IET Power Electron.*, Vol. 10, No. 8, pp. 875-883, Jun. 2017.

[26] S. J. Huang, S. H. Dai, J. L. Su, and T. S. Li, "Design of a contactless power supply system with dual output capability for AGV applications," in *IEEE Glob. Conf. Consum. Electron., GCCE*, pp. 1-3, 2017.

[27] S. H. Chang, P. Y. Chen, Y. H. Ting, and S. W. Hung, "Robust current control-based sliding mode control with simple uncertainties estimation in permanent magnet synchronous motor drive systems," *IET Electr. Power Appl*., Vol. 4, No. 6, pp. 441-450, Jul. 2010.

[28] C. Y. Xia, W. Wang, G. P. Chen, and X. J. Wu, "Robust control for the relay ICPT system under external disturbance and parametric uncertainty," *IEEE Trans. Contr. Syst. Technol*., Vol. 25, No. 6, pp. 2168-2175, Nov. 2017.

[29] Y. Li, Y. X. Zhang, Q. X Yang, and Z. Yan, "Analysis and experimental validation on maximum power and efficiency in wireless power transfer system via coupled magnetic resonances," *Diangong Jishu Xuebao*, Vol. 31, No. 2, pp. 18-24, Jan. 2016.
[30] X. D. Wang, M. C. Yang, J. F. Liu, and Y. Yu, "Transient analysis of contactless excitation systems with relative rotating pot core transformers," *Proc. the CSEE*, Vol. 35, No. 22, pp. 5915-5923, Nov. 2015.
[31] T. Imura, "Study on maximum air-gap and efficiency of magnetic resonant coupling for wireless power transfer using equivalent circuit," in *IEEE Int. Symp. Ind. Electron*., pp. 3664-3669, 2010.

Jinfeng Liu was born in Heilongjiang, China. She received her B.S. and M.S. degrees in Electrical and Information Engineering from North East Agriculture University, Harbin, China, in 2001 and 2004, respectively. She received her Ph.D. degree in Electrical Engineering from the Harbin University of Science and Technology, Harbin, China, in 2011, where she is presently working as an Associate Professor. Her current research interests include motor control, distribution systems and resonance compensation.

Kun Li was born in Heilongjiang, China. He received his B.S. degree in Electrical Engineering from Shijiazhuang Tiedao University, Hebei, China, in 2015; and his M.S. degree in Electronics and Communication Engineering from the Harbin University of Science and Technology, Harbin, China, in 2019. His current research interests include DC-DC converters and ICPT systems.

Ningzhi Jin was born in Harbin, China. He received his B.S., M.S. and Ph.D. degrees in Electrical Engineering from the Harbin University of Science and Technology, Harbin, China, in 2003, 2006 and 2012, respectively. He is presently working as an Associated Professor of power electronics and power drives at the Harbin University of Science and Technology. His current research interests include motor drives and power electronics.

Herbert Ho-Ching Iu was born in Hong Kong, China. He received his B.S. (Hons) degree in Electrical and Electronic Engineering from The University of Hong Kong, Hong Kong, China, in 1997. He received his Ph.D. degree in Electronic and Information Engineering from the Hong Kong Polytechnic University, Hong Kong, China, in 2000. He is presently working as a Professor at the University of Western Australia, Perth, WA, Australia. His current research interests include power electronics, renewable energy, nonlinear dynamics and memristors.